Electronic Supplementary Material (ESI) for Chemical Communications.

Electronic Supporting Information

Solid-state self-catalyzed growth of N-doped carbon tentacles on M(Fe, Co)Se surface for rechargeable Zn-air batteries

Pan Qi[a], Mengxu Chen[a], Teng Luo[a], Changjiu Zhao[a], Cong Lin[c], Hao Luo*[a,b], Dawei Zhang*[a]

[a]Anhui Province Key Laboratory of Advanced Catalytic Materials and Reaction Engineering, School of Chemistry and Chemical Engineering, Hefei University of Technology, Hefei, Anhui, 230009, China.

[b]Intelligent Manufacturing Institute of Hefei University of Technology, Hefei 230051, Anhui, China.

[c]Department of Mechanical Engineer, The Hong Kong Polytechnic University. Kowloon, 999077, Hong Kong, China.

*Corresponding authors: luohao@hfut.edu.cn; zhangdw@ustc.edu.cn

This file includes Experimental Section and Fig. S1-S18.

1. Experimental Section

1.1 Materials

Ferrous chloride tetrahydrate ($FeCl_2 \cdot 4H_2O$), cobalt chloride hexahydrate ($CoCl_2 \cdot 6H_2O$), nitrilotriacetic acid ($C_6H_9NO_6$), potassium hydroxide (KOH), selenium powder, zinc acetate dihydrate ($Zn(CH_3COO)_2) \cdot 2H_2O$), Pt/C (20 wt%), iridium dioxide (IrO_2), isopropanol, absolute ethanol, Ketjen black, and Nafion (5 wt%) were all purchased from Sigma-Aldrich company and used without further treatments.

1.2 Syntheses of M(Fe, Co)Se/NC

In a typical synthesis, 0.72 g cobalt chloride hexahydrate and 0.6 g nitrilotriacetic acid was firstly thoroughly ground for 30 min to obtain the desired precursor. Then, the prepared precursor was placed in a quartz boat downstream of a tube furnace while a quartz boat with 1.2 g selenium powder was placed upstream. The tube was heated to 700 ^oC under N_2 flow with a heating ramp of 6 ^oC min^{-1} and maintained at 700 ^oC for 2 h. After cooling to room temperature, black products were collected and marked as CoSe/NC. FeSe/NC were obtained following the same method except using ferrous chloride tetrahydrate rather than cobalt chloride hexahydrate.

1.3 Material characterizations

The material phase and crystallinity were analyzed by an X-ray diffractometer (XRD, Rigaku D/MAX2500VL/PC) while the material morphology was studied using

a field emission scanning electron microscope (SEM, Zeiss Gemini 500) and a field emission transmission electron microscope (TEM, JEOL JEM-2100F). The nitrogen absorption/desorption were tested on a gas adsorption instrument (Quantachrome Autosorb-IQ3), and the resulting isothermal curves were employed to determine the specific surface area and pore size distribution of the materials. The Raman characterization was conducted on a laser Raman spectrometer (HORIBA LabRAM HR Evolution) and the elemental types and chemical states of the materials were studied by an X-ray photoelectron spectrometer (XPS, ESCALAB 250Xi).

1.4 Electrochemical measurements

To prepare the working electrode, 5 mg synthesized material and 1 mg Ketjen black were mixed and ground, followed by dispersing in 1 mL deionized water and isopropanol solution (volume ratio of 4:1) containing 20 μL Nafion (5 wt%). The resulting black solution was then sonicated for 45 min to generate a homogeneous slurry. Finally, 3 μL slurry was evenly coated onto the polished glassy carbon surface and placed in air to form a uniformly loaded film.

The ORR and OER tests were performed in O_2-saturated 0.1 M KOH solution (O_2 injection for 45 min) with 1 M KCl-saturated calomel electrode and a Pt wire as the reference and counter electrode, respectively. The linear scanning voltammetry (LSV) was conducted with a scanning speed of 5 mV/ s, and the ORR and OER voltage sweep ranges were set to -0.7~0 V and 0~1 V, respectively. The ATA-1B rotary disc electrode (RDE) measurement was tested on the CHI604D electrochemical analyzer. The

reversible hydrogen electrode (RHE) test used following equation to calculate the potential: $V_{RHE} = V_{SCE} + V^{0}_{SCE} + 0.0592 * pH$, where V^{0}_{SCE} is 0.2415 V at room temperature. For the ORR test using RDE, the number of transferred electrons (n) was calculated by the Koutechy-Levich (K-L) equation, i.e., $1/J = 1/J_L + 1/J_K = 1/B\omega^{1/2} + 1/J_K$ ($B = 0.2nFC_0D_0^{2/3}V^{-1/6}$), where J, J_K, and J_L are current density, kinetic density, and diffusion limit current density, respectively, ω is the rotational angular velocity, V is the viscosity of the electrolyte (0.01 $cm^2\ s^{-1}$ for 0.1 M KOH solution), and F, C_0, and D_0 are the Faraday constant (96485 C mol^{-1}), O_2 concentration (1.2×10^{-6} mol cm^{-3}), and the oxygen diffusion coefficient (1.93×10^{-5} $cm^2\ s^{-1}$), respectively.

The material performance in liquid zinc-air battery was tested through a home-made battery with 6M KOH + 0.2M $Zn(CH_3COO)_2$ as the electrolyte. Typically, 8 mg catalyst material was completely dispersed by sonication for 30 min in a solvent composed of 60 μL Nafion (5 wt%), 200 μL isopropanol, and 740 μL deionized water. Then 125 μL catalyst ink was uniformly coated onto a one-square-centimeter carbon cloth so that the mass loading was 1 mg/cm^2. All the zinc-air batteries were tested under the same experimental conditions.

2. Supporting Figures

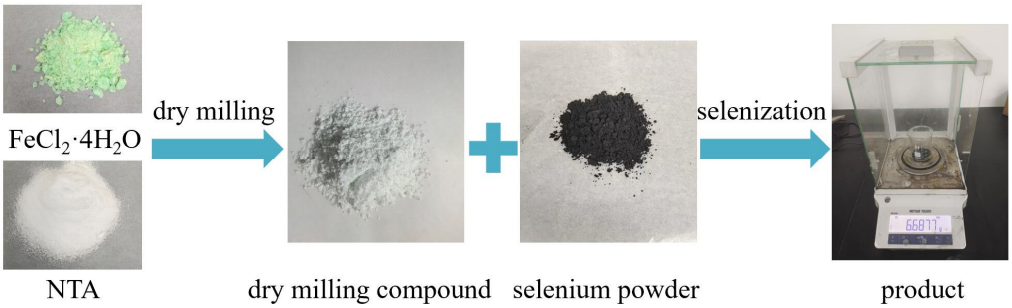

Fig. S1 Scheme for scale-up synthesis of FeSe/NC catalyst, showing the weight of corresponding product.

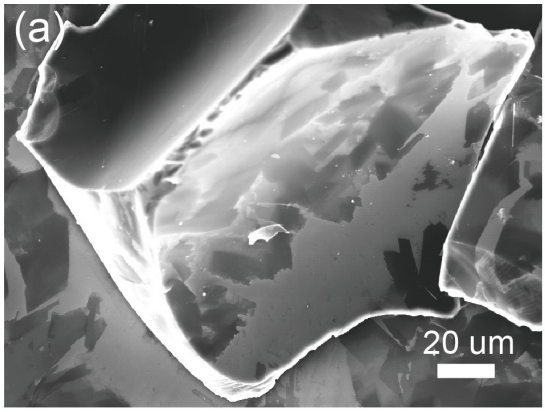

(c) Se-NC

Element	Weight %
C	86.65%
N	4.89%
O	3.03%
Se	5.44%

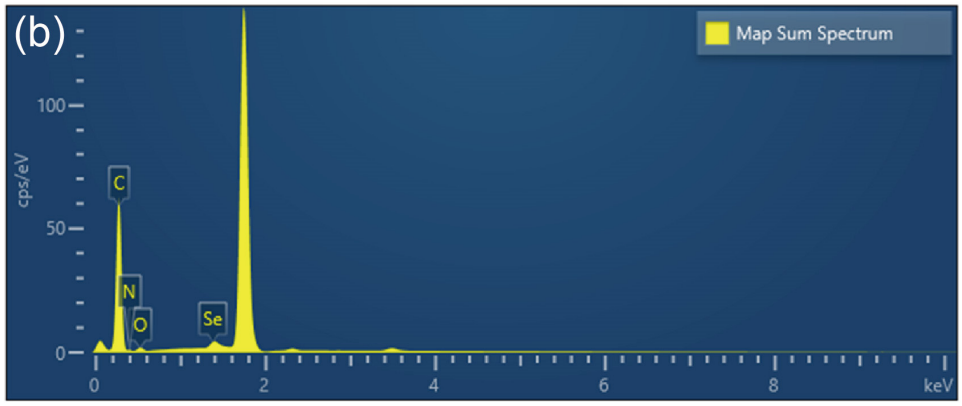

Fig. S2 (a) SEM image, (b) EDS spectrum, and (c) elemental quantification of the Se-NC (pyrolyzed product using NTA and Se power as the precursors).

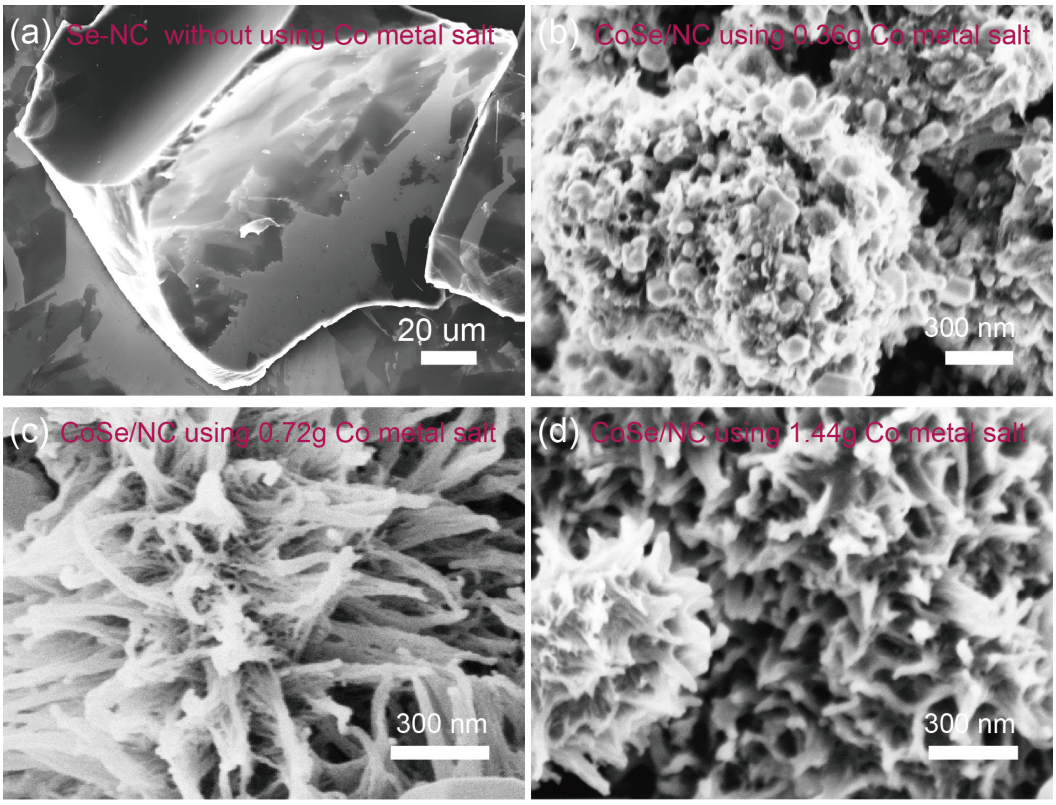

Fig. S3 SEM images of (a) Se-NC without Co salt, (b) CoSe/NC using 0.36 g Co salt, (c) CoSe/NC using 0.72 g Co salt, and (d) CoSe/NC using 1.44 g Co salt.

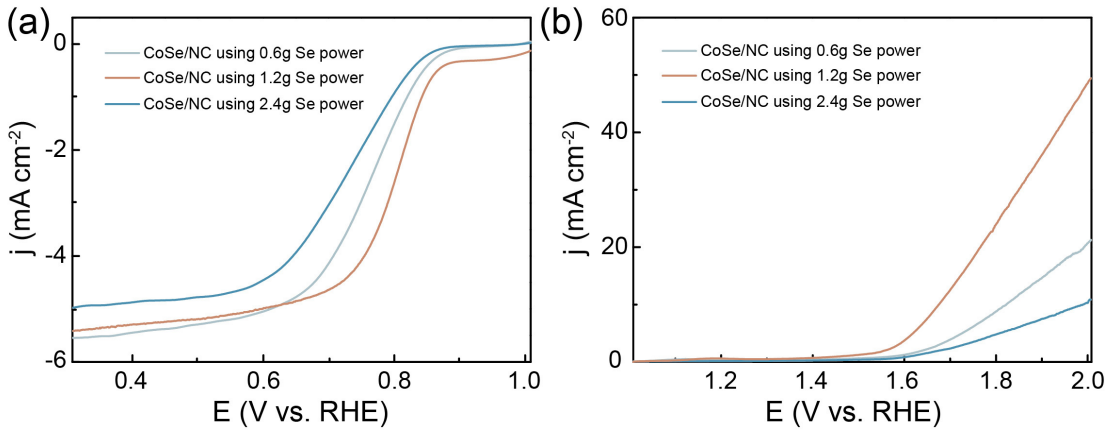

Fig. S4 LSV curves record at 1600 rpm of CoSe/NC catalysts with different amounts of Se power, showing the ORR and OER activity.

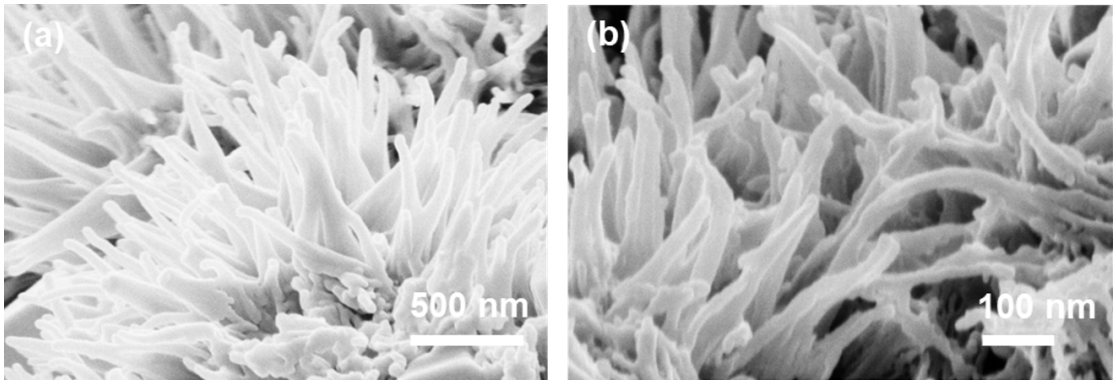

Fig. S5 SEM images of the CoSe/NC.

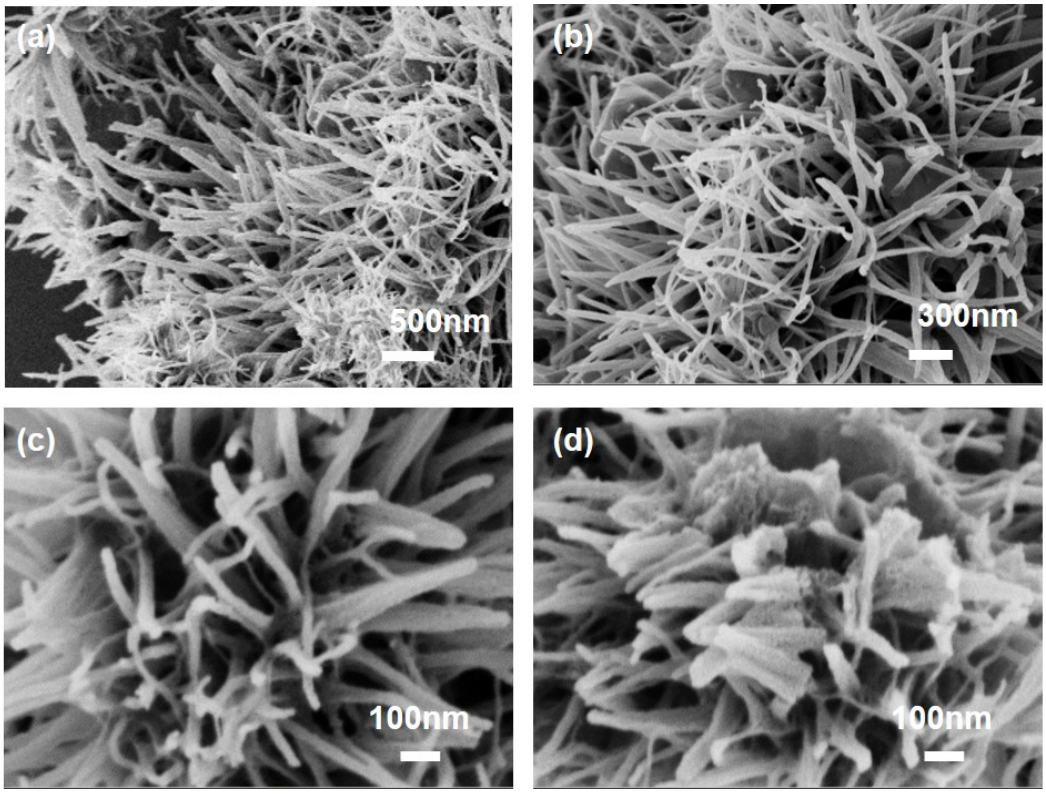

Fig. S6 SEM images of the FeSe/NC.

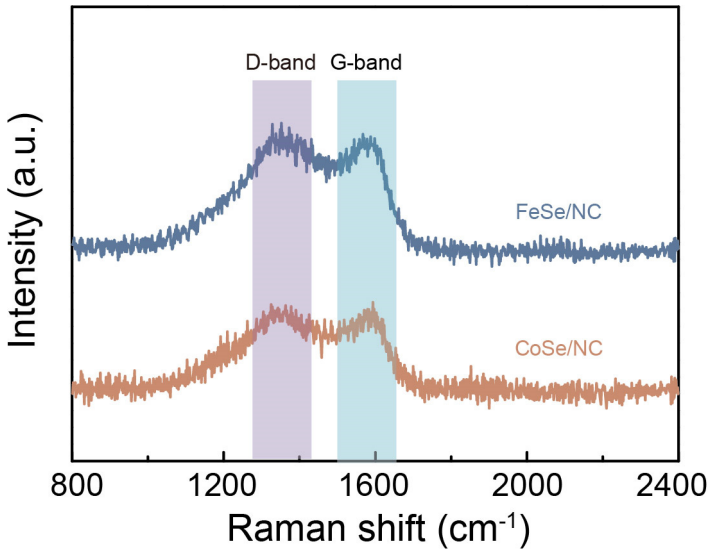

Fig. S7 Raman spectra of CoSe/NC and FeSe/NC.

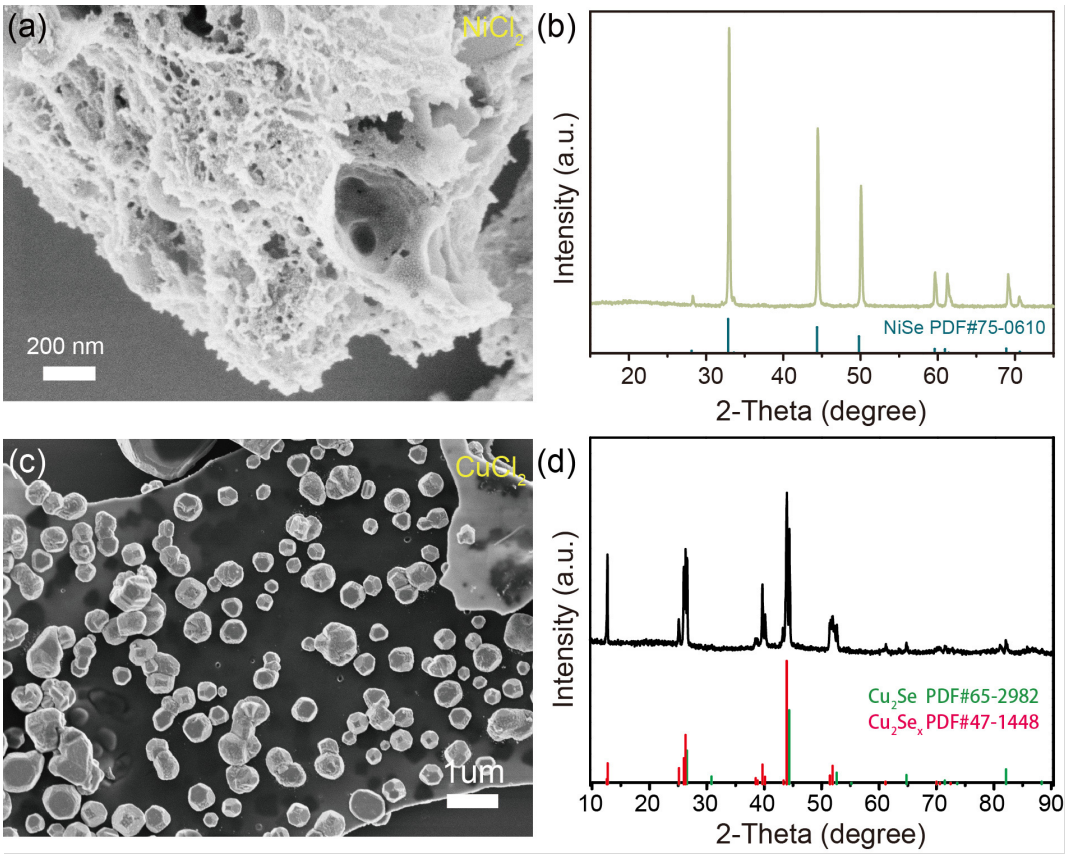

Fig. S8 (a, c) SEM images of the pyrolyzed products using $NiCl_2$ or $CuCl_2$. (b, d) XRD patterns of corresponding pyrolyzed products.

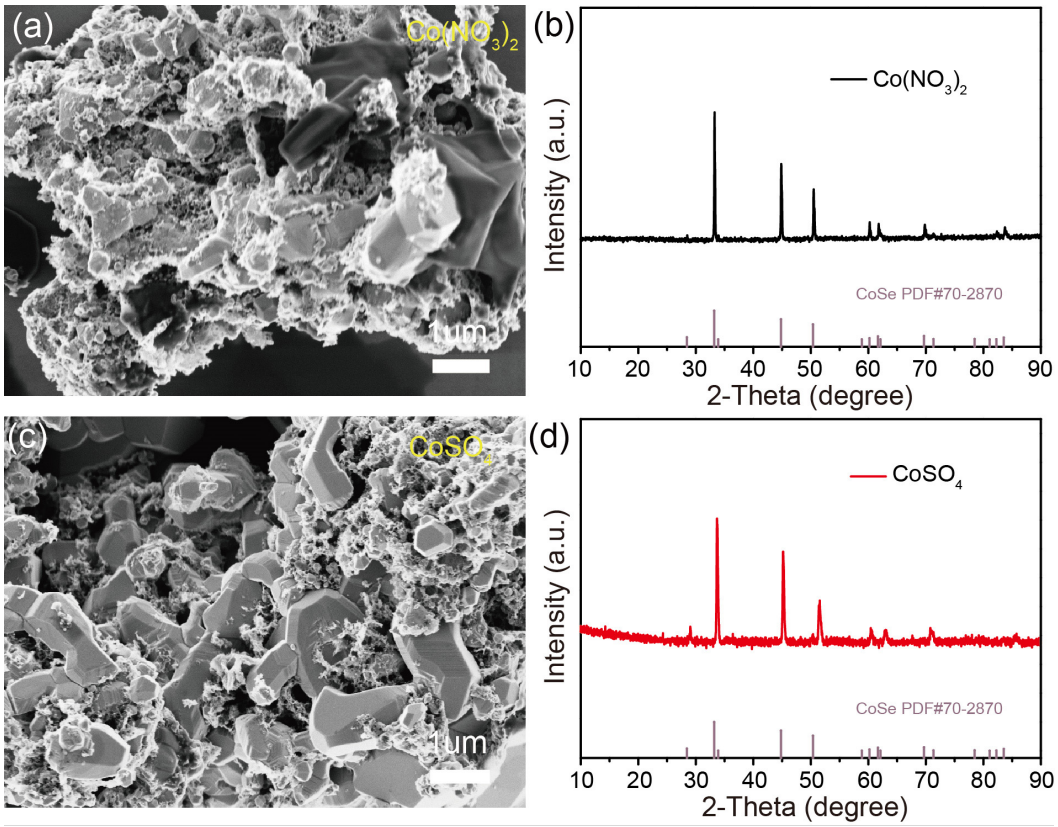

Fig. S9 (a, c) SEM images of the pyrolyzed products using $Co(NO_3)_2$ or $CoSO_4$. (b, d) XRD patterns of corresponding pyrolyzed products.

Additional description for Fig. S8 and S9

To simply investigate the formation mechanism of the carbon tentacles in CoSe/NC and FeSe/NC, we have conducted a series of additional comparative syntheses using other metal salts instead of $CoCl_2$ while keeping other conditions unchanged. These alternative metal salts include $NiCl_2$, $CuCl_2$, $Co(NO_3)_2$, and $CoSO_4$, and the results are shown in Fig. S8 and S9. The SEM images and XRD patterns in Fig. S8 indicate that although $NiCl_2$ and $CuCl_2$ can be used to prepare NiSe and $CuSe_x$, they are unable to catalyze the carbon tentacles growth on their surface, which proves the effect of Co and Fe ions in catalyzing the carbon tentacles. In addition, the SEM images and XRD patterns in Fig. S9 show that $Co(NO_3)_2$ and $CoSO_4$ can lead to the successful preparation of CoSe, but they can not catalyze the carbon tentacles growth either. This indicates that chloride anions also play a critical role in the formation of the carbon tentacles.

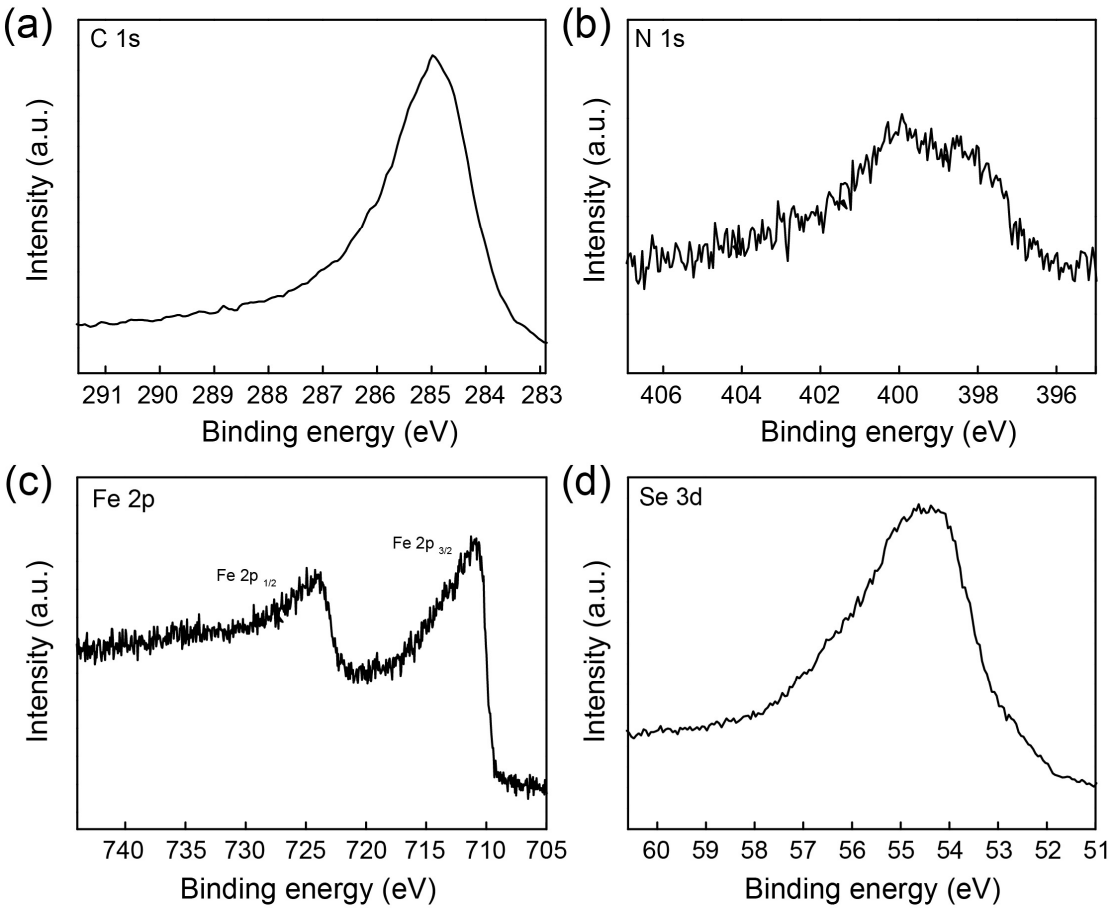

Fig. S10 (a) C 1s, (b) N 1s, (c) Fe 2p, and (d) Se 3d XPS spectra of FeSe/NC.

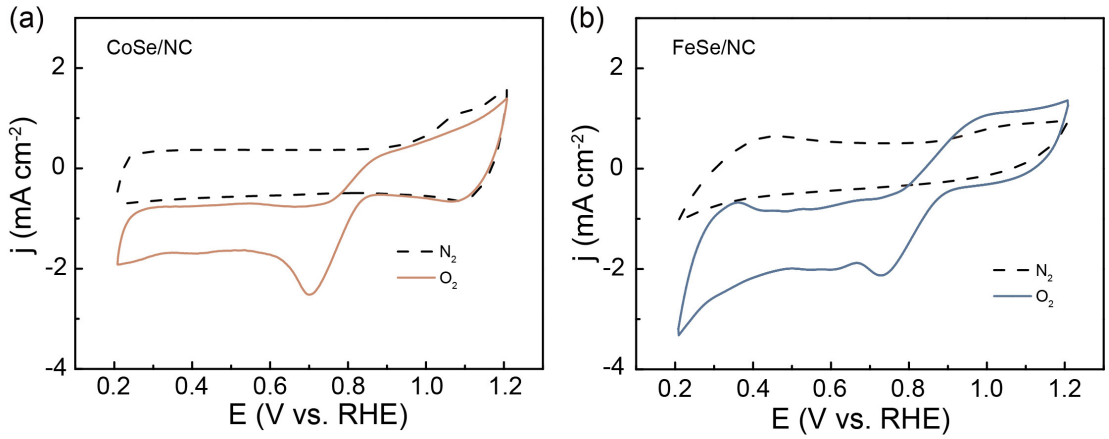

Fig. S11 CV curves of (a) CoSe/NC and (b) FeSe/NC in N_2- or O_2-saturated 0.1M KOH solution.

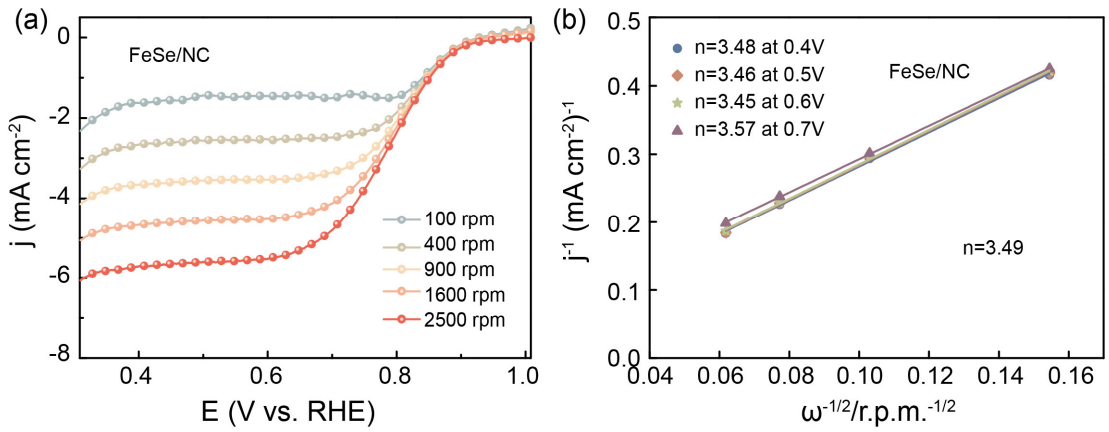

Fig. S12 (a-b) LSV curves of FeSe/NC at various rotation speeds and its corresponding K-L plots at various potentials and the calculated electron transfer number.

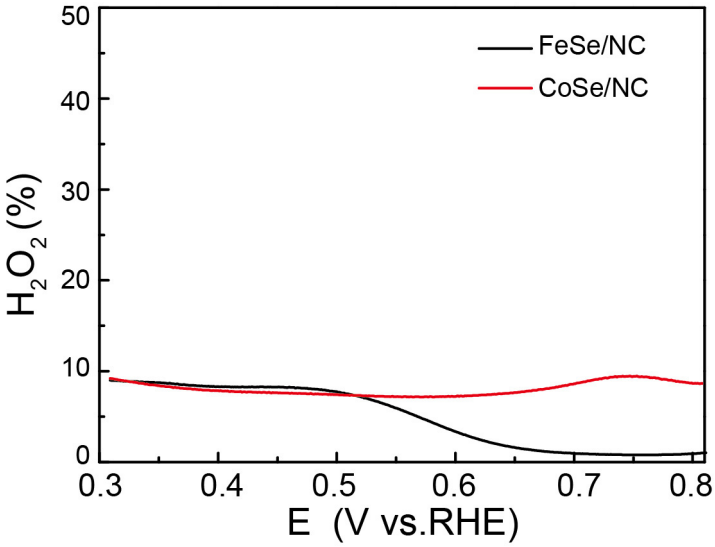

Fig. S13 H_2O_2 yield recorded with RRDE at a scan rate of 10 mV s^{-1} and rotation speed of 1600 rpm.

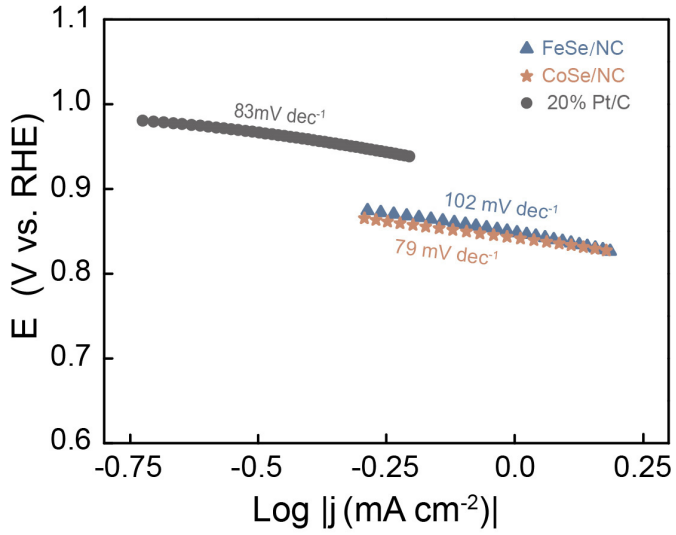

Fig. S14 Tafel plots of CoSe/NC, FeSe/NC, and Pt/C.

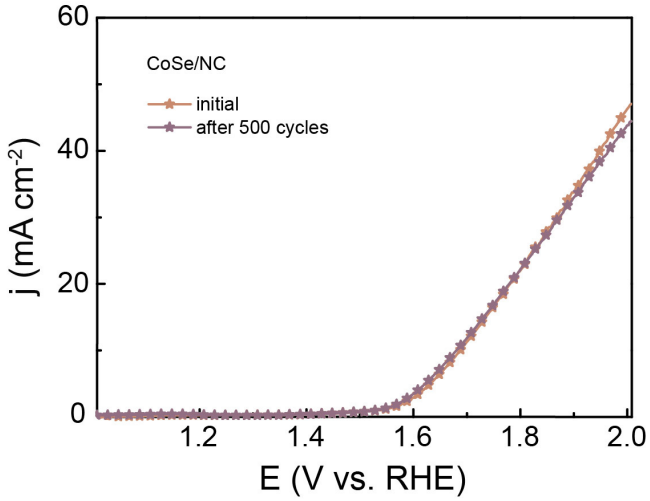

Fig. S15 LSV curves of CoSe/NC for the OER before and after 500 CV cycles.

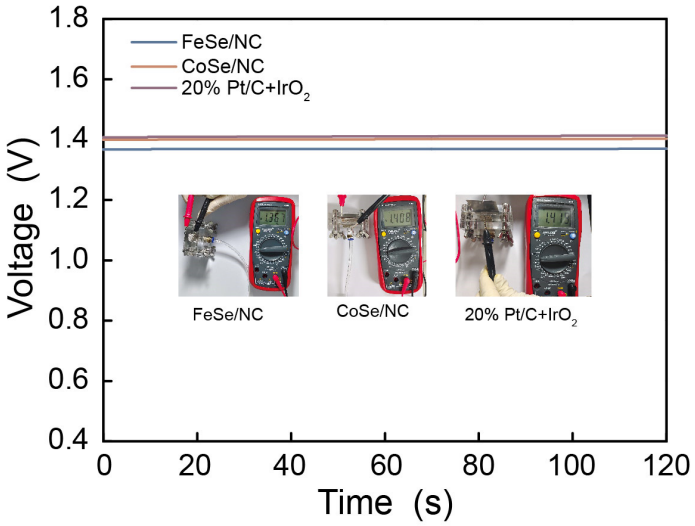

Fig. S16 Open-circuit voltage of the Zn-air batteries based on CoSe/NC, FeSe/NC, and 20%Pt/C+IrO_2 (inset: direct voltage observation).

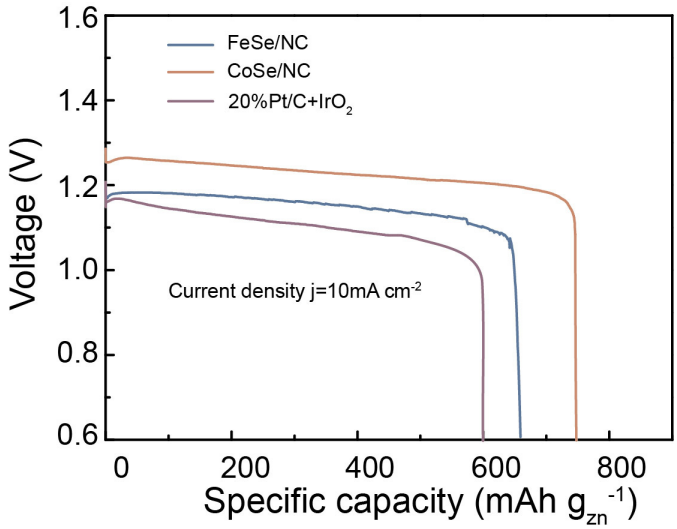

Fig. S17 Specific capacities of the Zn-air batteries using CoSe/NC, FeSe/NC, and 20%Pt/C+IrO_2.

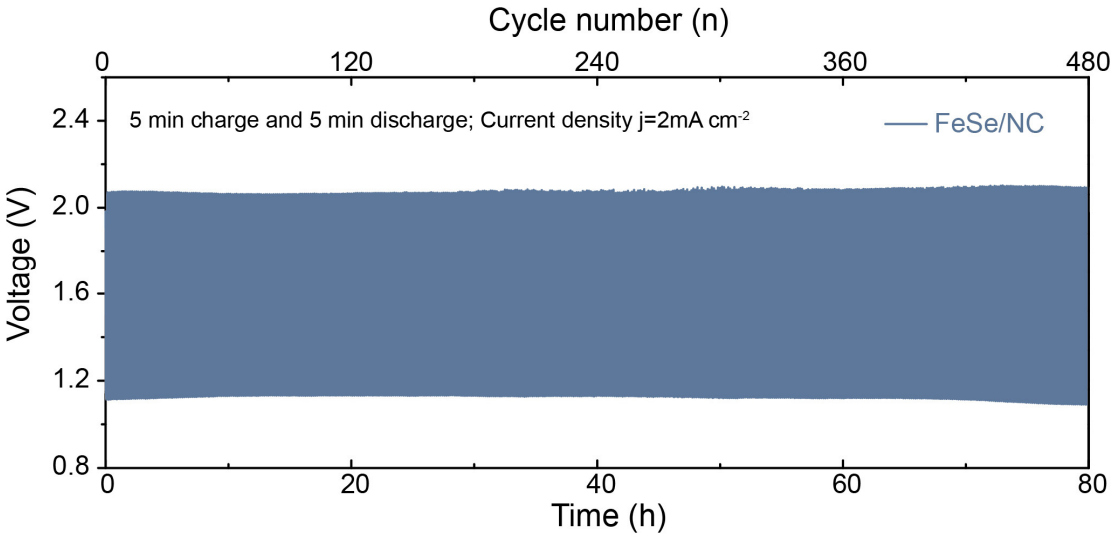

Fig.S18 Cycling stability of the FeSe/NC-based Zn-air battery at a discharge/charge current density of 2 mA/cm^2.

3. Supporting Table

Table S1. Performance comparison of the Zn-air batteries based on CoSe/NC and reported Co-based materials.

ORR catalyst	Electrolyte	Peak power density ($mW\ cm^{-2}$)	Reference
NSC/Co_9S_8-200	6 M KOH+0.2M $Zn(AC)_2$	176	Nano Energy, 2022, 92, 106750
Co/$CoSe_2$@CN_X	6 M KOH+0.2M $Zn(AC)_2$	113.2	J. Mater. Chem. A, 2023, 11, 5179-5187
$CoSe_2$@NC	6 M KOH+0.2M $Zn(AC)_2$	137.1	Nano Energy, 2022, 91, 106675
CoNP@FeNC-0.05	6 M KOH+0.2M $Zn(AC)_2$	104.4	Nano-Micro Lett., 2022, 14, 162
P-$CoSe_2$/C@CC	6 M KOH+0.2M $Zn(AC)_2$	124.4	J. Colloid Interface Sci., 2023, 633, 424-431
Co_{40}SAs/AC@NG	6 M KOH+0.2M $Zn(AC)_2$	221	Adv. Funct. Mater., 2023, 33, 2209736
H-Co@Fe/N/C	6 M KOH+0.2M $Zn(AC)_2$	125.2	Appl. Catal., B, 2020, 278, 119259
Co@hNCTs-800	6 M KOH+0.2M $Zn(AC)_2$	149	Nano Energy, 2020, 71, 104592
CoSe/NC	**6 M KOH+0.2M $Zn(AC)_2$**	**154**	**This work**